Centrality-dependent direct photon p_t spectra in Au + Au collisions at the BNL Relativistic Heavy Ion Collider (RHIC) energy $\sqrt{s_{NN}} = 200$ GeV

Fu-Ming Liu,[1,*] Tetsufumi Hirano,[2] Klaus Werner,[3] and Yan Zhu[1]

[1]*Institute of Particle Physics, Central China Normal University, Wuhan, People's Republic of China*

[2]*Department of Physics, University of Tokyo, 113-0033, Japan*

[3]*Laboratoire SUBATECH, University of Nantes, IN2P3/CNRS, Ecole des Mines, Nantes, France*

(Received 29 December 2007; revised manuscript received 12 August 2008; published 28 January 2009)

We calculate the centrality dependence of transverse momentum (p_t) spectra for direct photons in Au + Au collisions at the BNL Relativistic Heavy Ion Collider (RHIC) energy $\sqrt{s_{NN}} = 200$ GeV, based on a realistic data-constrained (3 + 1)-dimensional hydrodynamic description of the expanding hot and dense matter, a reasonable treatment of the propagation of partons and their energy loss in the fluid, and a systematic study of the main sources of direct photons. The resultant p_t spectra agree with recent PHENIX data in a broad p_t range. The competition among the different direct photon sources is investigated at various centralities. Parton energy loss in the plasma is considered for photons from fragmentation and jet-photon conversion, which causes about 40% decrease in the total contribution. In the high p_t region, the observed R_{AA} of photons is centrality independent at the accuracy of 5% based on a realistic treatment of energy loss. We also link the different behavior of R_{AA} for central and peripheral collisions, in the low p_t region, to the fact that the plasma in central collisions is hotter than that in peripheral ones.

DOI: 10.1103/PhysRevC.79.014905 PACS number(s): 25.75.−q, 12.38.Mh

I. INTRODUCTION

The formation and observation of a quark-gluon plasma (QGP) in heavy ion collisions are important goals of modern nuclear physics [1,2]. Suppression of high p_t hadron yields [3] is one of the most important features observed at the BNL Relativistic Heavy Ion Collider (RHIC). Theoretically this is attributed to the interaction between jets (hard partons) and the bulk matter [4–7]. Experimentally, absence of the suppression in d + Au collisions [8] reveals that the suppression results from a final-state effect and, in turn, that the hot and dense matter is created in Au + Au collisions. The amount of suppression depends significantly on the centrality of the collision [9], which implies that various sizes of hot dense matter are formed in heavy ion collisions at various centralities. This offers us an excellent opportunity to study the interaction of partons inside the system and, consequently, properties of the matter under extreme conditions.

Hadron production in heavy ion collisions involves bulk hadronization of the thermal partons at low p_t, the fragmentation of quenched hard partons at high p_t, and the hadronization contributed from both thermal and hard partons at intermediate p_t. However, it is quite difficult to systematically describe all these hadronization processes, since some of them are beyond the perturbative treatment and usually contain many parameters without full understanding. Low p_t hadrons also strongly interact with each other after hadronization and cannot carry *direct* information from inside the hot matter. Under this situation, a systematic study of direct photons in a wide range of transverse momentum and centrality can serve as a guide to understanding the whole reaction processes of heavy ion collisions, since we do not need to treat hadronization itself nor interaction between produced direct photons and the bulk matter thanks to the large mean free path of direct photons compared to the typical size of the system in heavy ion collisions. Competition among different sources at various centralities may be also useful in understanding the production mechanism of direct photons.

In this paper, we first study the role of jet quenching on the centrality dependence of direct photon production. For this purpose, a reliable treatment of hard parton energy loss is needed. This is formulated via the Baier-Dokshitzer-Mueller-Peigné-Schiff (BDMPS) framework [7] and tested on pion suppression at various centralities. Since neutral pions and other mesons are significantly suppressed in central Au + Au collisions, and since the suppression has an evident centrality dependence, the following question arises naturally: What is the role of hard parton energy loss on direct photon production? The main purpose of this paper is to answer this question.

We also investigate the interplay among the various sources of direct photons. Similar to hadron suppression, photons from parton fragmentation are expected to offer information on the interaction between hard partons and the bulk via jet quenching. Thermal photons and photons from parton-bulk interactions are penetrating probes of the hot matter, respectively, through interaction of partons inside bulk matter and interaction between primary partons and the bulk matter. It is interesting to see whether one reproduces the observed photon spectra by considering all photon sources simultaneously and consistently at different collision centralities. By identifying the dominant sources of direct photons at given values of p_t, we will be able to discuss in which way the different p_t regions of the photon spectra provide information about the different production processes.

We need a realistic description of the hot and dense matter to investigate the effect of bulk matter on photon emission. This

*liufm@iopp.ccnu.edu.cn

is achieved by using three-dimensional (3D) hydrodynamic simulations of bulk matter [10,11] which have already been tested against a vast body of low p_t hadron data at RHIC.

To perform a systematic study of *direct* photon production (from sources other than neutral meson decays) in relativistic heavy ion collisions, we shortly review the possible sources in the following.

Primordial NN scattering. The direct photon production via Compton scattering and quark-antiquark annihilation can be calculated in perturbation theory using the conventional parton distribution functions and the factorization hypothesis. In principle one should also consider at this stage higher order contributions, such as bremsstrahlung of photons accompanying, for example, two-jet production in hard parton-parton scattering. However, we consider this component as a part of the so-called jet fragmentation (or bremsstrahlung) contribution to be affected by the thermalized matter, which we will discuss separately.

Thermal photons. In high energy nuclear collisions, the density of secondary partons is so high that the quarks and gluons rescatter and eventually thermalize to form a bubble of hot QGP. The plasma expands, cools down, and goes through a phase transition to hadronic gas (HG) phase. Thermal photons can be produced during the whole history of the evolution of hot matter from the QGP phase to the HG phase through the mixed phase because of collisions of or radiations from thermalized particles. Yields of photons from a thermal source are exponentially damped so that contribution to the very high p_t region is negligible. However, contribution to low p_t is expected to be dominant in central collisions in which the size and temperature of a hot and dense matter are large enough.

Jet-photon conversion. When hard partons pass through thermalized matter, they may interact. Collisions between jets and deconfined partons via quark-antiquark annihilation and quark-gluon Compton scattering can produce direct photons. This is often called jet-photon conversion.

Jet fragmentation. Photon production also occurs as a higher order effect in purely partonic initial hard scatterings: at any stages of the evolution of a jet (final-state parton emission), there is a possibility of emitting photons. Existence of a QGP again affects the results of fragmented photons, since energetic partons lose their energy prior to fragmentation. In this work, we assume fragmentation of partons only outside the plasma, which is similar to high p_t hadron production from jet fragmentation.

There are possible contributions to photon production which are not included in the present study. Naively, the medium-induced photon radiation is expected mainly at the low transverse momentum region, since several photon (or gluon) emissions share the lost energy of the hard parton which is only a minor part of the total hard parton energy according to the sample-averaged results. However, due to the event-by-event fluctuation, the medium-induced photon radiation may contribute to the high transverse momentum region. In an early study [12], it is shown that this contribution is much lower than jet-photon conversion at low and intermediate p_t and much lower than fragmentation at high p_t, while in a later study [13], it is shown that this contribution is not so small. Such contributions were also studied by Zakharov [14]. In this paper, we neglect it and leave it at that. In the time interval between the primordial collisions at $\tau = 0$ and the thermalization of the hot matter at τ_0, the interaction between nonequilibrated soft partons and hard partons may also produce direct photons. We do not know how to treat this contribution exactly. Some previous work tried to estimate it with different initial times and showed that this contribution may be negligible, because this time interval is much shorter than the lifetime of the equilibrated matter ($\sim$20 fm/c, c.f. Fig. 1). So this contribution is also ignored in this paper.

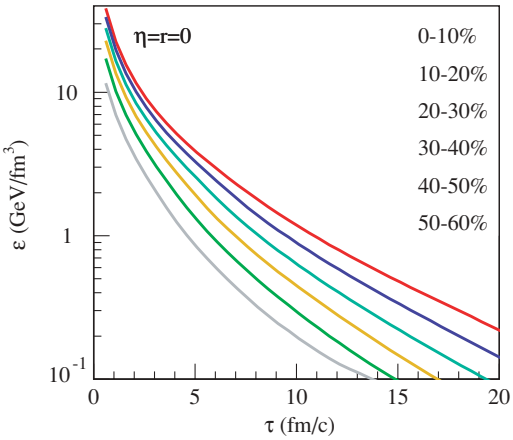

FIG. 1. (Color online) Time evolution of energy density at the center $(x, y, \eta) = (0, 0, 0)$ for various centrality. Each line from top to bottom corresponds to 0–10%, 10–20%, . . . , and 50–60% centrality, respectively.

The paper is organized as follows. In Sec. II, we first give a brief review of the space-time evolution of the hot matter created in Au + Au collisions at different centralities based on a (3 + 1)-dimensional ideal hydrodynamic calculation. In Sec. III, we discuss parton energy loss in the QGP. We investigate neutral pion production in the high p_t region in order to fix the parameters of the energy loss scheme. We discuss sequentially the contributions from various sources to direct photon p_t spectra in Sec. IV. We show our results and compare them with recent experimental data in Sec. V. Section VI is devoted to conclusions of the present study.

II. SPACE-TIME EVOLUTION OF THE HOT AND DENSE MATTER

Several sources of direct photon production in heavy ion collisions depend on the bulk dynamics of hot and/or dense matter and the matter along trajectories of energetic partons. So a realistic description of reaction dynamics is indispensable for the quantitative analysis of photon production. In our calculation, fully three-dimensional (3D) ideal hydrodynamics [10,11] is employed to describe the space-time evolution of the hot and dense matter created in Au + Au collisions at RHIC energy $\sqrt{s_{NN}} = 200$ GeV at various centralities. We solve the equations of energy-momentum conservation

$$\partial_\mu T^{\mu\nu} = 0 \tag{1}$$

in full 3D space (τ, x, y, η) under the assumption that the local thermal equilibrium is reached (maintained) at (after) an initial time $\tau_0 = 0.6$ fm/c. Here τ and η are the proper time and the space-time rapidity, respectively. x and y are transverse coordinates. In the transverse plane, the centers of two colliding nuclei are located at $(x, y) = (b/2, 0)$ and $(-b/2, 0)$ before the collision at an impact parameter b. Ideal hydrodynamics is characterized by the energy-momentum tensor

$$T^{\mu\nu} = (e + P)u^\mu u^\nu - Pg^{\mu\nu}, \tag{2}$$

where e, P, and u^μ are energy density, pressure, and local four-velocity, respectively. We neglect the finite net-baryon density, which is small near the midrapidity at RHIC. For the high temperature ($T > T_c = 170$ MeV) QGP phase, we use the equation of state (EOS) of massless noninteracting parton gas (u, d, s quarks and gluons) with a bag pressure B:

$$p = \tfrac{1}{3}(e - 4B). \tag{3}$$

The bag constant is tuned to be $B^{\frac{1}{4}} = 247.19$ MeV to match the pressure of the QGP phase to that of a hadron resonance gas at critical temperature $T_c = 170$ MeV. A hadron resonance gas model at $T < T_c$ includes all hadrons up to the mass of the $\Delta(1232)$ resonance. Our hadron resonance gas EOS implements chemical freeze-out at $T_{\rm ch} = T_c = 170$ MeV, as observed in collisions at RHIC [15]. This is achieved by introducing appropriate temperature-dependent chemical potentials $\mu_i(T)$ for all hadronic species i in a way that their numbers $\tilde{N}_i$ including all decay contributions from higher lying resonances, $\tilde{N}_i = N_i + \sum_R b_{R\to iX} N_R$, are conserved during the evolution [11,16–20]. Here N_i is the average multiplicity of the ith hadron species, and $b_{R\to iX}$ is the effective branching ratio (a product of branching ratio and degeneracy) of a decay process $R \to i + X$. In this partial chemical equilibrium (PCE) model [11], only strongly interacting resonances with large decay widths (whose decays do not alter $\tilde{N}_i$) remain chemically equilibrated below $T_{\rm ch}$. It should be noted that the hadronic chemical composition described by hydrodynamics using the PCE model is roughly consistent with that of the hadronic cascade models [21], as long as the latter are initialized at $T_{\rm sw} = 169$ MeV with thermal and chemical equilibrium distributions.

We assume that at $\tau_0 = 0.6$ fm/c, the initial entropy distribution is proportional to a linear combination of the number density of participants (85%) and binary collisions (15%) [21]. Centrality dependence of charged particle multiplicity observed by PHOBOS [22] has been well reproduced by full 3D hydrodynamics simulations with the above setups [21]. In the following calculations, hydrodynamic outputs at representative impact parameters $b = 3.2, 5.5, 7.2, 8.5, 9.7,$ and 10.8 fm are chosen for 0–10%, 10–20, ..., 50–60% centrality, respectively.

So far, the space-time evolution of the QGP fluid obtained as above has been also exploited for a quantitative study of hard and rare probes such as azimuthal jet anisotropy, nuclear modification factor of identified hadrons, disappearance of back-to-back jet correlation, and J/ψ suppression [23].

TABLE I. Initial temperature at the plasma center at initial time $\tau_0 = 0.6$ fm/c for various centralities.

Centrality (%)	0–10	10–20	20–30	30–40	40–50	50–60
T_0 (MeV)	370	357	341	327	301	272

In Table I, initial temperatures at the plasma center, $T_0 = T(\tau_0, 0, 0, 0)$, are shown for various centralities. These temperature values will be important to interpreting the centrality dependence of the slope of p_t spectra from thermal radiation, which will be discussed later. Figure 1 shows the time evolution of energy density at the center of fluids $(x, y, \eta) = (0, 0, 0)$ for various centralities. Clearly, for any given proper time τ, one obtains higher energy densities at the plasma center for the more central collisions.

For convenience of the following calculations, we introduce $f_{\rm QGP}(\tau, x, y, \eta)$ as the fraction of the QGP phase in a fluid element. It is obvious that $f_{\rm QGP} = 1$ (0) in the QGP (hadronic) phase. In the mixed phase, the fraction of the QGP is calculated via

$$f_{\rm QGP}\, e_{\rm QGP} + (1 - f_{\rm QGP}) e_{\rm had} = e(\tau, x, y, \eta),$$

with $e_{\rm QGP}$ and $e_{\rm had}$ being the energy densities of the QGP phase and the hadron phase at $T = T_c$, respectively.

III. PARTON ENERGY LOSS IN A PLASMA

Energy loss of hard partons in a plasma affects both jet-photon conversion and jet fragmentation. The momentum distribution of jets (energetic gluons or quarks with different flavors) from primordial nucleus-nucleus scattering is calculated as [24]

$$\frac{dN^{AB\to\rm jet}}{dy\, d^2p_t} = KT_{AB}(b) \sum_{abcd} \int dx_a\, dx_b\, G_{a/A}(x_a, M^2) \times G_{b/B}(x_b, M^2) \frac{\hat{s}}{\pi} \frac{d\sigma}{d\hat{t}}(ab \to cd)\delta(\hat{s} + \hat{t} + \hat{u}), \tag{4}$$

where $T_{AB}(b)$ is the nuclear overlapping function at an impact parameter b for each centrality, $G_{a/A}(x_a, M^2)$ and $G_{b/B}(x_b, M^2)$ are parton distribution functions in nuclei A and B. We take the Martin-Roberts-Stirling-Thorne leading-order (LO) parton distributions in the proton [25]. The elementary cross sections for $ab \to cd$ can be found in Ref. [24]. We set the factorization scale M and renormalization scale Q to be $M = Q = p_t$. $K = 2$ is chosen to take into account higher order contributions. These parameters are chosen to reproduce high p_t pion data in pp collisions at RHIC, which will be discussed later. The above formula for p_t spectra was extensively tested in pp ($p\bar{p}$) collisions in an energy range from $\sqrt{s} = 27.4$ to 630 GeV. The nuclear shadowing effect and EMC effect are taken into account through EKS98 scale dependent nuclear ratios $R_a^{\rm EKS}(x, A)$ [26]. Isospin of a nucleus with mass A, neutron number N, and proton number Z is corrected as follows:

$$G_{a/A}(x) = \left[\frac{N}{A} G_{a/N}(x) + \frac{Z}{A} G_{a/P}(x)\right] R_a^{\rm EKS}(x, A). \tag{5}$$

The isospin mixture and nuclear shadowing eventually cause a decrease of nuclear modification at the high p_t region, which will be shown in Sec. V.

We assume that all jets are produced at $\tau = 1/Q \approx 0$ with the phase-space distribution

$$f_0(\vec{p}, \vec{r}) \propto \frac{dN}{d^3p} T_A\left(x - \frac{b}{2}, y\right) T_B\left(x + \frac{b}{2}, y\right) \delta(z), \quad (6)$$

where $\vec{r} = (x, y, z)$ is the coordinate of a jet, b is the impact parameter, and T_A and T_B are thickness functions of nuclei A and B. The δ function reflects the highly Lorentz-contracted colliding nuclei A and B. The phase-space distribution of hard partons is normalized as

$$\int f_0(\vec{p}, \vec{r})\, d^3r = (2\pi)^3 \frac{dN}{d^3p}. \quad (7)$$

Energetic partons can suffer interactions with the fluid and lose their energies. We employ the BDMPS formula [6] to calculate parton energy loss in a plasma created in heavy ion collisions. For a parton of type $i = q, g$ with initial momentum $\vec{p}_0$ formed at $\vec{r}_0$, the whole path length of a parton traversing the expanding QGP (including the mixed phase) is

$$L(\vec{p}_0, \vec{r}_0) = \int_{\tau_0}^{\infty} d\tau\, \theta(f_{\rm QGP}(\tau, \boldsymbol{x}(\tau))). \quad (8)$$

Here $\boldsymbol{x}(\tau)$ is a trajectory of a parton, $f_{\rm QGP}(\tau, \boldsymbol{x}(\tau))$ is the fraction of the QGP phase at a position $(\tau, \boldsymbol{x}(\tau))$, and θ is a step function, which gives $\theta(f_{\rm QGP})$ equal unity in the QGP and the mixed phases and zero in the hadron phase.

The total energy loss along this path is calculated as

$$\Delta E(i, \vec{p}_0, \vec{r}_0) = D \int_{\tau_0}^{\infty} d\tau \epsilon(i, \tau, \boldsymbol{x}(\tau))\, \theta(f_{\rm QGP}(\tau, \boldsymbol{x}(\tau))). \quad (9)$$

Here D is an adjustable parameter, and $\epsilon(i, \tau, \boldsymbol{x}(\tau))$ is the energy loss per unit distance for a parton i at a position $(\tau, \boldsymbol{x}(\tau))$, given as [6]

$$\epsilon(i, \tau, \boldsymbol{x}(\tau)) = \alpha_s \sqrt{\mu^2 E^*/\lambda_i}.$$

Here, the temperature-dependent running coupling constant—assuming a similar formula as the lowest order one in perturbation theory—can be obtained by fitting the numerical results from lattice quantum chromodynamics (QCD) simulations [27] as

$$\alpha_s(T) = \frac{6\pi}{(33 - 2N_f)\ln(8T/T_c)}. \quad (10)$$

The Debye screening mass is given as $\mu = gT$, with $g^2/4\pi = \alpha_s(T)$. The energy of a hard parton in the local rest frame is $E^* = p^\mu u_\mu$, where p^μ is the four-momentum of the hard parton in the laboratory frame and u_μ is a local fluid velocity. All hard partons are treated as on-shell massless particles. The mean free path λ_i of a parton i is given as

$$\lambda_g^{-1} = \sigma_{gq}\rho_q f_{\rm QGP} + \sigma_{gg}\rho_g f_{\rm QGP}, \quad (11)$$

$$\lambda_q^{-1} = \sigma_{qq}\rho_q f_{\rm QGP} + \sigma_{qg}\rho_g f_{\rm QGP}, \quad (12)$$

with cross sections $\sigma_i = C_i \alpha_s \pi / T^2$ [28]. The color factors $2C_i$ are 4/9, 1, and 9/4 for qq, qg, and gg scattering, respectively. The parton densities ρ_q and ρ_g are obtained from the EOS of the massless relativistic gas. The fraction of the QGP phase $f_{\rm QGP}$ is considered in the mixed phase to ensure a smooth transition from the QGP phase to the HG phase. Note that the above quantities, i.e., temperature T, fluid velocity u_μ, parton densities ρ_i, and, in turn, mean free path λ_i, depend on the location of the parton $\boldsymbol{x}(\tau)$ and can be obtained from full 3D hydrodynamics simulations discussed in the previous section.

Various sizes of the plasma are formed in heavy ion collisions at different centralities. We use the common energy loss formula Eq. (9) for all of these media. The main purpose in the present paper is a systematic study of direct photon production rather than a detailed analysis of parton energy loss. So we allow ourselves to introduce an adjustable parameter D in Eq. (9) to fit simultaneously the neutral π-meson data in Au + Au collisions at different centralities [9].

We first discuss pion production in proton-proton collisions. We calculate neutral π-meson production assuming pQCD factorization, Eq. (4),

$$\frac{dN_{pp}^{\pi^0}}{dy\, d^2p_t} = \sum_{c=g,q_i} \int dz_c \frac{dN^{pp\to c}}{dy\, d^2p_t{}^c} \frac{1}{z_c^2} D^0_{\pi^0/c}(z_c, Q^2), \quad (13)$$

where $D^0_{\pi^0/c}(z_c, Q^2)$ is π^0 fragmentation functions parametrized by Kniehl *et al.* [29]. In Fig. 2, p_t spectra for neutral pions in pp collisions at $\sqrt{s} = 200$ GeV calculated with $M = Q = 2p_t$, p_t, and $p_t/2$ are compared to PHENIX data [30]. In the high p_t region where the pQCD is expected to work, we reasonably reproduce the experimental data with the above setup with $K = 2$ and $M = Q = p_t$. We use the p_t spectrum as a reference spectrum in the following calculations.

The effect of parton energy loss is taken into account through the medium modified fragmentation function $D_{\pi^0/c}(z_c, Q^2, \Delta E_c)$ which describes suppression of neutral pion yields as

$$\frac{dN_{AB}^{\pi^0}}{dy\, d^2p_t} = \sum_{c=g,q_i} \int dz_c \frac{dN^{AB\to c}}{dy\, d^2p_t{}^c} \frac{1}{z_c^2} D_{\pi^0/c}(z_c, Q^2, \Delta E_c), \quad (14)$$

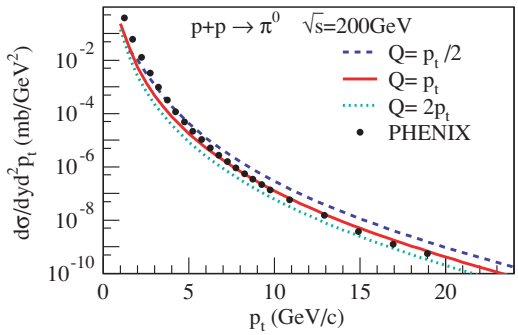

FIG. 2. (Color online) Neutral pion production in pp collisions at $\sqrt{s} = 200$ GeV is compared to PHENIX data [30]. Three lines from top to bottom correspond to $Q = p_t/2$, p_t, and $2p_t$, respectively.

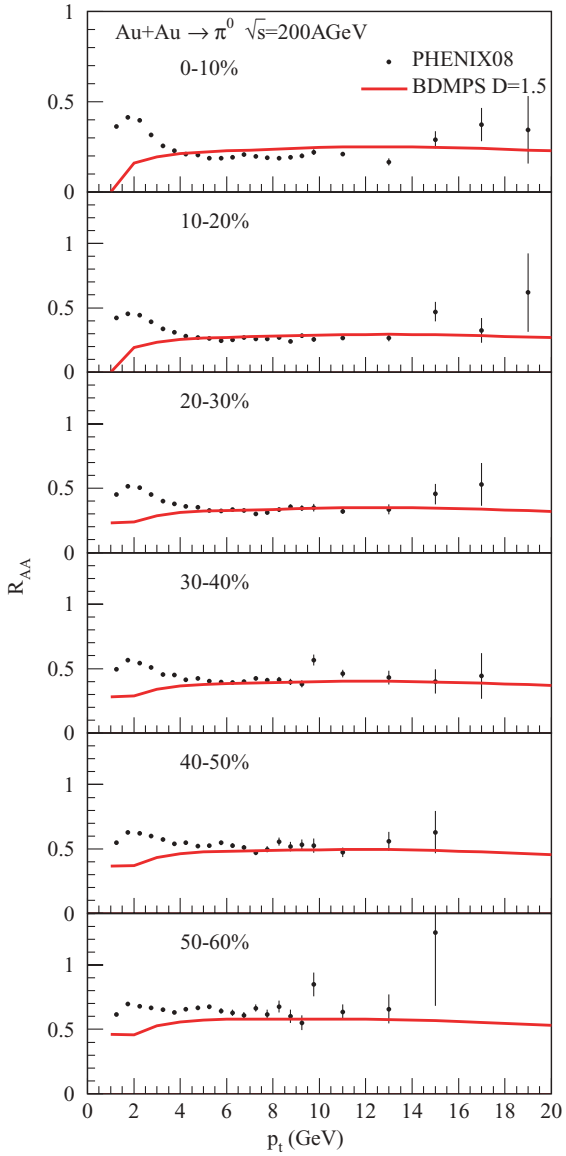

FIG. 3. (Color online) Nuclear modification factors of π^0. Solid lines are calculated with the BDMPS energy loss formula with amplified parameter $D = 1.5$ (see text for details). Plots are PHENIX data [9].

with [31]

$$D_{\pi^0/c}(z_c, Q^2, \Delta E_c) = \left(1 - e^{-\frac{L}{\lambda_c}}\right)\left[\frac{z_c'}{z_c} D^0_{\pi^0/c}(z_c', Q^2) + \frac{L}{\lambda_c}\frac{z_g'}{z_c} D^0_{\pi^0/g}(z_g', Q^2)\right] + e^{-\frac{L}{\lambda_c}} D^0_{\pi^0/c}(z_c, Q^2). \quad (15)$$

Figure 3 shows the nuclear modification factors for neutral pions in Au + Au collisions at $\sqrt{s_{NN}} = 200$ GeV for different centralities. Solid lines are results with an energy loss parameter $D = 1.5$, and plots are the PHENIX data [9]. With a common value of the parameter $D = 1.5$, we can reasonably reproduce the π^0 yields in the high p_t region at all centralities simultaneously. It should be noted that in the PHENIX data [9], a ∼10% normalization error and ∼7–16% errors (depending on centrality) due to $N_{\rm coll}$ are omitted in Fig. 3. In the region $p_t < 5$ GeV/c, our results undershoot the experimental data owing to the absence of neutral pion production from bulk components in this calculation. Notice that low p_t pion data have already been described well [21] by using hydrodynamic simulations employed in the present study. In the following photon calculations, we always use the BDMPS energy loss formula (9) with $D = 1.5$.

IV. DIFFERENT SOURCES OF DIRECT PHOTON PRODUCTION

Leading order contribution. Similar to Eq. (4), the leading order contribution to direct photon production in nucleus-nucleus collisions reads

$$\frac{dN^{AB\to\gamma}}{dy\, d^2p_t} = T_{AB}(b) \sum_{ab} \int dx_a\, dx_b\, G_{a/A}(x_a, M^2) \times G_{b/B}(x_b, M^2) \frac{\hat{s}}{\pi}\frac{d\sigma}{d\hat{t}}(ab \to \gamma + X) \times \delta(\hat{s} + \hat{t} + \hat{u}), \quad (16)$$

where the elementary processes $ab \to \gamma + X$ are Compton scattering $qg \to \gamma q$ and annihilation $q\bar{q} \to g\gamma$.

Fragmentation contribution. Higher order contributions in pp collisions are due to jet fragmentation. We can calculate them as

$$\frac{dN^{\rm frag}_{pp}}{dy\, d^2p_t} = \sum_{c=g,q_i} \int dz_c \frac{dN^{pp\to c}}{dy\, d^2p_t{}^c} \frac{1}{z_c^2} D^0_{\gamma/c}(z_c, Q^2), \quad (17)$$

with photon fragmentation functions $D^0_{\gamma/c}(z, Q^2)$ being the probability for obtaining a photon from a parton c which carries a fraction z of the parton's momentum. So $p_t{}^c = p_t/z_c$ is the transverse momentum carried by the parton c before fragmentation, and $d^3p/E = z_c^2 d^3p^c/E^c$. The effective fragmentation functions for obtaining photons from partons can be calculated perturbatively. We use the parametrized solutions by Owens [24].

In heavy ion collisions, parton energy loss in a plasma should be taken into account. This can be done via modified fragmentation functions [31]

$$D_{\gamma/c}(z_c, Q^2, \Delta E_c) = (1 - e^{-\frac{L}{\lambda_c}})\left[\frac{z_c'}{z_c} D^0_{\gamma/c}(z_c', Q^2) + \frac{L}{\lambda_c}\frac{z_g'}{z_c} D^0_{\gamma/g}(z_g', Q^2)\right] + e^{-\frac{L}{\lambda_c}} D^0_{\gamma/c}(z_c, Q^2), \quad (18)$$

with $z_c' = p_t/(p_t{}^c - \Delta E_c)$ and $z_g' = (L/\lambda_c)\, p_t/\Delta E_c$ being the rescaled momentum fractions carried by the parton c and the emitted gluons before fragmentation. λ_c is mean free path of the parton c in the plasma, and L is the path length of each parton traversing the plasma defined in Eq. (8). Thus, in heavy ion collisions, contributions from fragmentation become

$$\frac{dN^{\rm frag}_{AB}}{dy\, d^2p_t} = \sum_{c=g,q_i} \int dz_c \frac{dN^{AB\to c}}{dy\, d^2p_t{}^c} \frac{1}{z_c^2} D_{\gamma/c}(z_c, Q^2, \Delta E_c). \quad (19)$$

This formula counts only fragmented photons outside the plasma. In principle, when fragmentation into photons happens inside the plasma, the photon can escape the plasma due to the long mean free path. However, it is not evident when and where fragmentation happens.

Thermal production. The emission rate of photons is $\Gamma = E\,d^3R/d^3p$, where R is the number of photons emitted from a medium per unit space-time volume with temperature T. Total yields of thermal photons can be obtained by summing the emission rate over the space-time volume as

$$\frac{dN^{\rm thermal}}{dy\,d^2p_t} = \int d^4x\Gamma(E^*,T), \tag{20}$$

with $d^4x = \tau\,d\tau\,dx\,dy\,d\eta$ and $E^* = p^\mu u_\mu$ being the photon energy in the local rest frame. Here, $p^\mu = (p_t\cosh y, p_t\cos\phi, p_t\sin\phi, p_t\sinh y)$ is the photon's four-momentum in the laboratory frame and u_μ is a local fluid velocity. In our calculations, the thermal photon emission rate covers both contributions from the QGP phase and the hadronic phase

$$\Gamma(E^*,T) = f_{\rm QGP}\Gamma^{\rm QGP\to\gamma}(E^*,T) + (1-f_{\rm QGP})\Gamma^{\rm HG\to\gamma}(E^*,T), \tag{21}$$

where $f_{\rm QGP}$ and T are the fraction of the QGP phase and temperature of the fluid, respectively, both being obtained in the hydrodynamic simulations. In this formula, we calculate thermal photon production above the thermal freeze-out temperature $T_{\rm th} = 100$ MeV. The photon emission rate from $2\to2$ processes between thermal partons, i.e., the QCD Compton process $qg\to\gamma q$ and annihilation $q\bar q\to g\gamma$, was first calculated with the hard thermal loop resummation technique [32,33]. Later, the Landau-Pomeranchuk-Migdal (LPM) interference effect for emitted photons turned out to be important [34], leading to

$$\Gamma^{\rm QGP\to\gamma}(E^*,T) = \sum_{i=1}^{N_f}\left(\frac{e_i}{e}\right)^2\frac{\alpha\alpha_S}{2\pi^2}T^2\frac{1}{e^x+1}\left[\ln\left(\frac{\sqrt{3}}{g}\right)+\frac{1}{2}\ln(2x) + C_{22}(x)+C_{\rm brems}(x)+C_{\rm ann}(x)\right], \tag{22}$$

with $x = E^*/T$ and

$$C_{22}(x) = \frac{0.041}{x} - 0.3615 + 1.01e^{-1.35x}, \tag{23}$$

$$C_{\rm brems}(x)+C_{\rm ann}(x) = 0.633x^{-1.5}\ln(12.28+1/x) + \frac{0.154x}{(1+x/16.27)^{0.5}}.$$

In the calculation, we take $N_f = 3$ and a temperature-dependent running coupling as in Eq. (10).

Thermal photon emission in the hadronic phase results from interactions such as $\pi\pi\to\rho\gamma$, $\pi\rho\to\pi\gamma$, and $\rho\to\pi\pi\gamma$. Interactions of mesons or baryons with strangeness can also produce photons, but the contributions are relatively small because of the phase-space suppression resulting from their heavier masses. In our work, the photon emission rate from the hadronic phase is based on the massive Yang-Mills (MYM) calculation [35], where photon production from mesons with strangeness has been included as well as the axial meson a_1 as an exchanging particle for nonstrange initial states. Hadrons are composite objects, so form factors are considered to simulate finite hadronic size effects [36].

Jet-photon conversion with jet energy loss. When hard partons propagate in a plasma, they also collide with thermal partons and produce direct photons via the Compton process and the quark-antiquark annihilation. We call this process jet-photon conversion, since it is a conversion of a jet into a photon with almost the same momentum as that of the originating jet parton. Contribution from the jet-photon conversion is calculated by integrating the conversion rate over the space-time evolution of the hot and dense matter in the QGP phase:

$$\frac{dN^{\rm jpc}}{dy\,d^2p_t} = \int\Gamma^{\rm jpc}(E^*,T)f_{\rm QGP}(x,y,\eta,\tau)\,d^4x. \tag{24}$$

The photon production rate by annihilation and Compton scattering of hard partons in the medium can be approximated as [37,38]

$$\Gamma^{\rm jpc}(E^*,T) = \frac{\alpha\alpha_s}{4\pi^2}\sum_q e_q^2 f_q(\vec p,x)T^2\left[\ln\frac{4E_\gamma^*T}{m_{\rm th}^2} - C\right], \tag{25}$$

where E^* is the photon energy in the local rest frame, $C = 2.323$, $m_{\rm th}^2 = g^2T^2/6$, and the strong coupling $\alpha_s = g^2/4\pi$ is temperature dependent as in Eq. (10). α is the electromagnetic couplings, and e_q and $f_q(\vec p,x)$ are the electric charge and the phase-space density of a hard parton of flavor q. The phase-space distribution of hard partons at τ is obtained by considering parton energy loss as

$$f(\vec p,x) = f(\vec p,\vec r,\tau) = \int d^3p_0 f_0(\vec p_0,\vec r-\vec v t)\delta(\vec p_0-\vec p-\vec v\Delta E),$$

where $f_0(\vec p,\vec r)$ is the phase-space distribution at $\tau = 0$ described in Eqs. (6) and (7). The δ-function expression reflects the energy loss of a parton moving along a straight-line trajectory with $\vec v \equiv \vec p/E = \vec p_0/E_0$. ΔE is the energy loss from τ_0 to τ and calculated as in Eq. (9) but replacing the upper limit of integral ∞ with τ.

V. RESULTS AND DISCUSSION

In Fig. 4, the calculated p_t spectra of direct photons in Au + Au collisions at $\sqrt{s_{NN}} = 200$ GeV at centralities 0–20% and 20–40% are compared with PHENIX data [41,42]. Here we sum over all contributions discussed in the previous section. The theoretical results for 0–20% centrality are obtained as a mixture of the calculations for 0–10% and 10–20% centrality with a weight of 50% each; a corresponding procedure applies for the 20–40% centrality results. The PHENIX data are reproduced within our multicomponent model remarkably well.

In Fig. 5, we show a detailed comparison of the calculated p_t spectra of direct photons with PHENIX data [42] for the centralities 0–10%, 10–20%, . . . , 50–60%. Again, our results agree with data very well in a broad range of p_t and centrality.

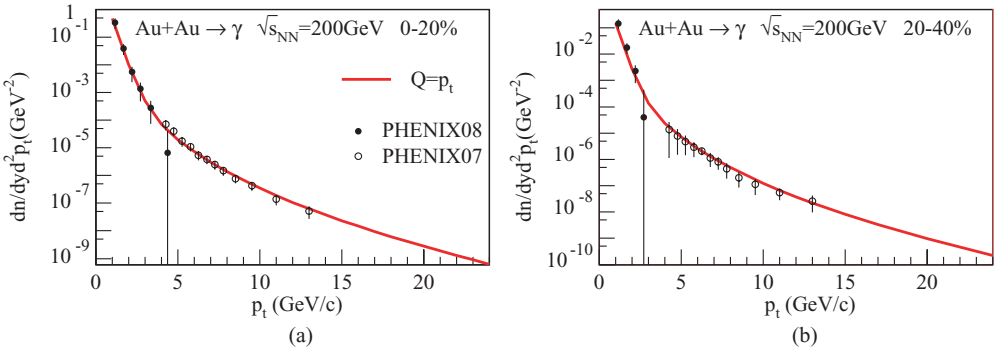

FIG. 4. (Color online) Direct photon production in Au + Au collisions at centrality 0–20% and 20–40%. PHENIX data are shown as open circles [42] and filled circles [41].

Since all the curves are almost parallel to each other, one gets more insight by using the nuclear modification factor R_{AA}, obtained by dividing a p_t spectrum in nucleus-nucleus collisions by the $N_{\rm coll}$-scaled p_t spectrum in pp collisions. In Fig. 6, we show the invariant differential cross section of direct photons in pp collisions. The calculation includes the leading order contribution plus fragmentation contribution, using a scale $Q = p_t$. PHENIX data are shown as open circles [42] and filled circles [41]. In high p_t regions, our result agrees with the data reasonably well; so we use it to calculate nuclear modification in Figs. 7 and 10. It also provides a baseline calculation with the LO contribution and fragmentation contribution in Au + Au collisions. Whereas, in low p_t regions where pQCD is not expected to work, our result undershoots the data slightly, although the error bars are large in the data. The dashed line is a fit to the measured differential cross section of direct photons in pp collisions at the RHIC energy $\sqrt{s} = 200$ GeV, that is,

$$\frac{d\sigma}{dy\,d^2p_t} = 0.01834\left(1+\frac{{p_t}^2}{1.432}\right)^{-3.27} \quad \text{mb/GeV}^2,$$

which is employed to calculate the nuclear modification factor from the thermal contribution in Fig. 11(a).

Figure 7 shows how the nuclear modification factor for direct photons, R_{AA}, depends on centrality and on energy loss. Data for 0–10% centrality are taken from Refs. [42] and [39]. Figure 7(a) shows centrality dependence of R_{AA} compared to the PHENIX data. The three curves are 0–10% (dotted line), 20–30% (solid line), and 40–50% (dash-dotted line). R_{AA} has a weak centrality dependence at the high p_t region. This result is consistent with the observed phenomenon [42] that the p_t-integrated (for $p_t > 6$ GeV/c) R_{AA} of direct photons is almost independent of collision centrality. Does this imply a very weak effect from jet quenching? Figure 7(b) answers this question (here for the most central collisions). Comparing calculations with (dotted line) and without energy loss (solid line), one finds a difference of up to 40%. So the effect of parton energy loss is quite visible in the p_t range between 4 and over 20 GeV/c. If we would do the R_{AA} calculations without energy loss, the difference between central and semiperipheral collisions would be about 20%, whereas the complete calculation gives the same result for all

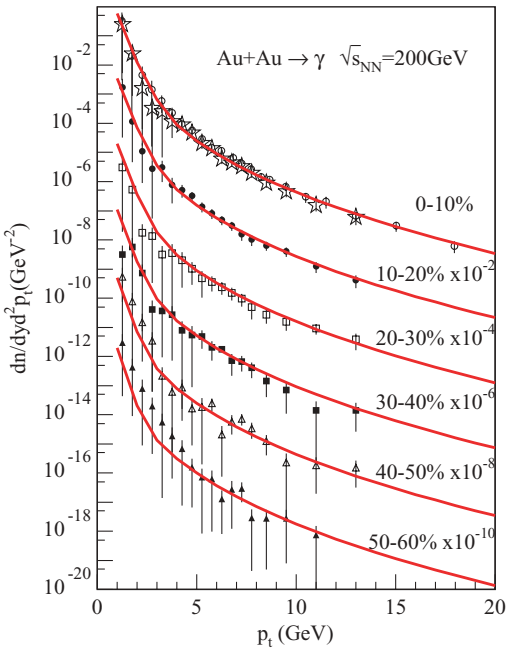

FIG. 5. (Color online) Direct photon production in Au + Au collisions at $\sqrt{s_{NN}} = 200$ GeV for different centralities (0–10%, 10–20%, . . . , 50–60%). Data were obtained by PHENIX [42].

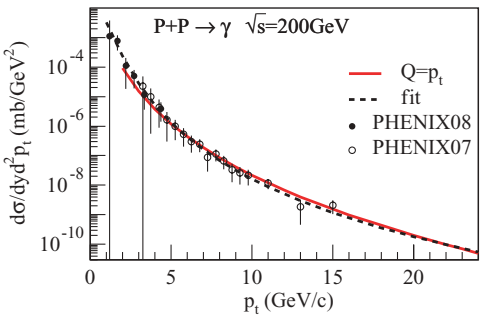

FIG. 6. (Color online) Invariant differential cross section of direct photons in pp collisions at $\sqrt{s} = 200$ GeV. Lines are leading order calculations plus fragmentation contributions, with a scale $Q = p_t$. PHENIX data are shown as filled circles [41] and open circles [42]. Dashed line is a fit to PHENIX data. See text for details.

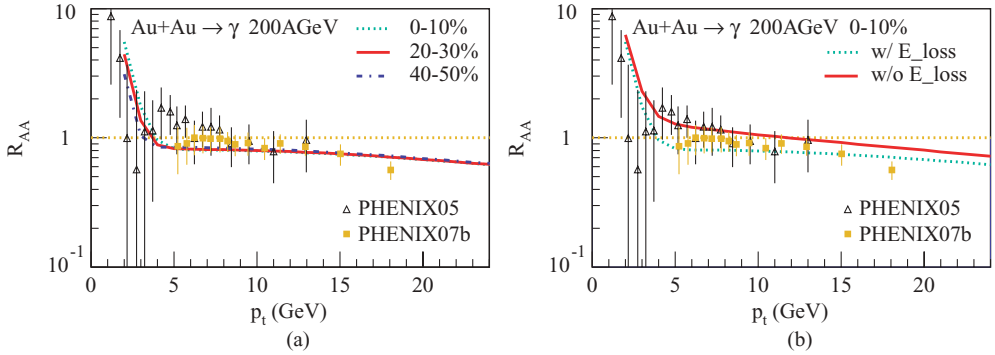

FIG. 7. (Color online) Nuclear modification factor of direct photons in Au + Au collisions R_{AA}. Data for 0–10% centrality are from Refs. [39,42]. (a) R_{AA} at centrality 0–10% (dotted line), 20–30% (solid line), and 40–50% (dash-dotted line). (b) R_{AA} at 0–10% centrality with energy loss (dotted line) and without energy loss (solid line).

centralities, within 5%. We have to admit that we are talking about small effects, requiring experimental data with relative errors of less than 5 to observe the effects.

To understand the above results, we look more closely at the different contributions. Parton energy loss in the plasma suppresses the fragmentation contributions and jet-photon conversion. So we study the ratios of the contribution with energy loss to the one without energy loss, as shown in Fig. 8 [(a) for fragmentation and (b) for jet-photon conversion]. Energy loss in the plasma depends on the path length of the hard parton inside the plasma, which in turn depends on the collision centrality. We do see a similar centrality dependence of the suppression for π^0 (jet quenching effect) in fragmentation contributions and jet-photon conversion.

To understand how these energy loss features affect the total contribution, we investigate the competition from different sources in Fig. 9, for the three centralities 0–10%, 20–30%, and 40–50%. The leading order (LO) contribution from primordial elementary scatterings is plotted as dotted lines, thermal contribution as dash-dotted lines, fragmentation contribution as dashed lines, and jet-photon conversion as solid lines. The latter two are calculated with parton energy loss in the plasma (left plots) and without (right). For all centralities, thermal photons dominate at low transverse momenta, and they are insignificant in the high p_t region. The LO contribution from primordial elementary scatterings dominates in the high p_t region. This contribution is independent of bulk volume.

Let us first discuss the central collisions. Here fragmentation and conversion are an order of magnitude smaller that the LO contribution. But from Fig. 9, we know that is due to the strong energy loss effect. Without this energy loss, these two contributions would be much bigger, and this is why we find a 40% difference between the total contribution with and without energy loss.

For peripheral collisions, without energy loss, the relative contribution from conversion is smaller than for central scatterings, since the the plasma region is smaller. But then also the suppression from energy loss is smaller for the peripheral than for the central collisions. So at the end, when including a proper energy loss treatment, for both central and peripheral collisions, conversion is roughly an order of magnitude smaller than the LO contribution, see Fig. 9(e). The relative contribution from fragmentation, without energy loss, is comparable in central and peripheral collisions; however, the energy loss is smaller in the latter ones. So fragmentation is somewhat more important in peripheral than in central collisions when

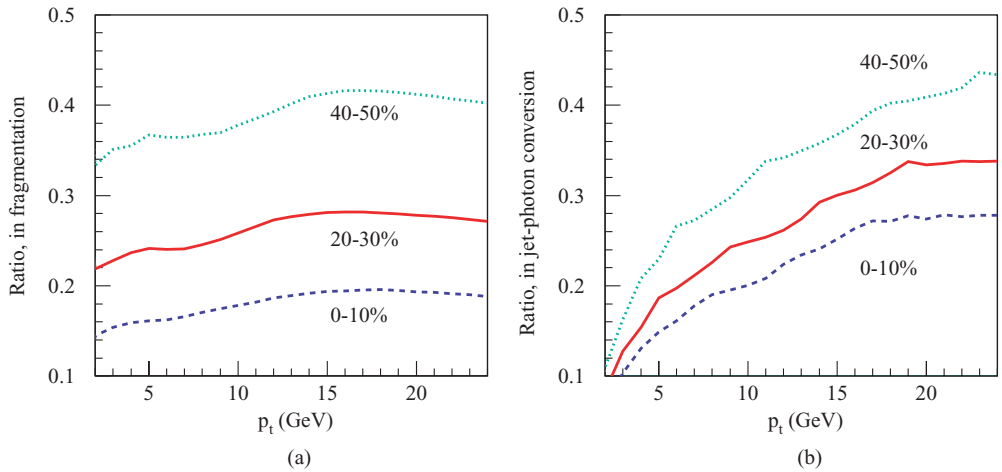

FIG. 8. (Color online) The ratio of the contribution with energy loss to the one without, in fragmentation (a) and jet-photon conversion (b).

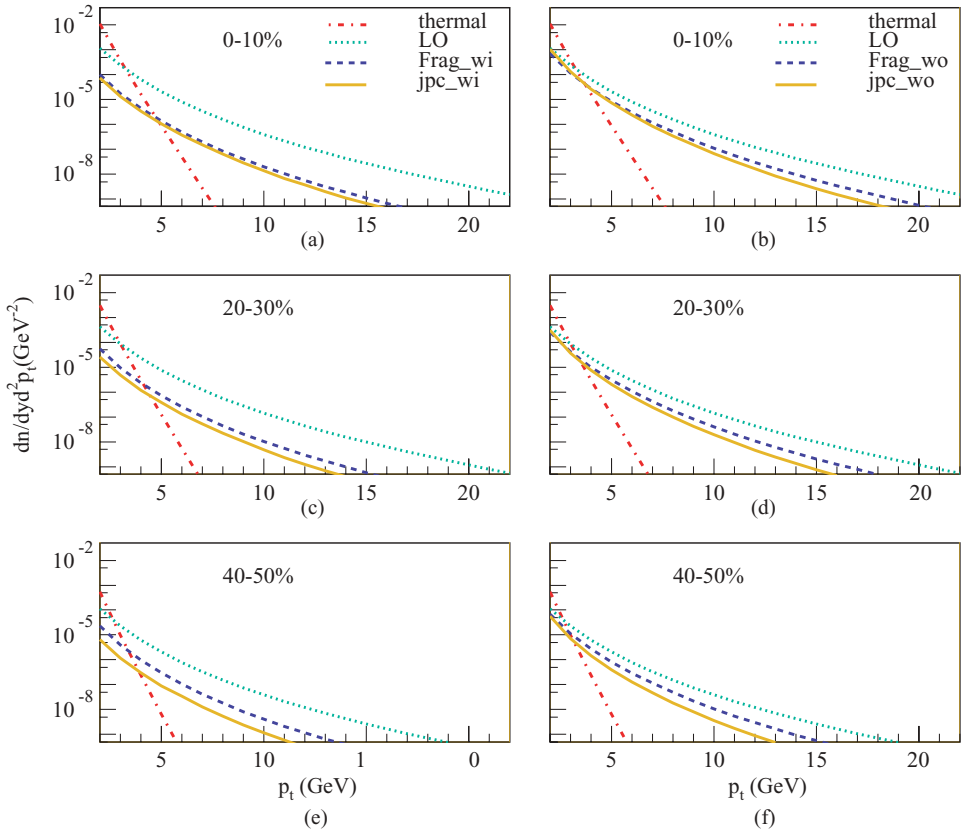

FIG. 9. (Color online) Competition among different sources for direct photon production in Au + Au collisions at $\sqrt{s_{NN}} =$ 200 GeV for different centralities. The leading order (LO) contribution from primordial elementary scatterings is plotted as dotted lines, thermal contribution as dash-dotted lines, fragmentation contribution as dashed lines and jet-photon conversion as solid lines.

energy loss is considered, as can be also seen from Fig. 10, which shows the contribution to R_{AA} from fragmentation and conversion for the different centralities: conversion contributes roughly 4% for all centralities, fragmentation between 5% (central) and 10% (peripheral).

At the end, R_{AA} is nearly centrality independent as shown in Fig. 7(a), but a realistic (and strong) partonic energy loss is needed to obtain this scaling behavior.

In the low p_t region, the thermal radiation contribution is of significant importance. We check the centrality dependence of the thermal contribution to R_{AA} in Fig. 11(a). At very low p_t, i.e., $p_t < 1$ GeV/c, the thermal contributions to R_{AA} at different centralities coincide with each other. However, the slope of R_{AA}^{thermal} changes and the dominant p_t region of thermal photons becomes smaller when one moves from central to peripheral collisions. This reflects the fact that the temperature in the core region depends on the collision centrality as shown in Table I in Sec. II.

So from the thermal source, the R_{AA} for central collisions exceed more and more the R_{AA} for peripheral collisions, which translates into a slight overshooting of the central total R_{AA} compared to the peripheral one, as seen in Fig. 8, in the region $p_t < 4$ GeV/c.

The fractions of thermal contribution as a function of p_t from different phases are shown in Fig. 11(b). Partial chemical equilibrium in the hadronic phase is used in this hydrodynamic simulation to keep the number of hadrons fixed below T_{ch}. If we ignore the contribution from particle decays and use a full chemical equilibrium (FCE), the photon emission rate from hadronic phase [35] can be used in this case. In case of

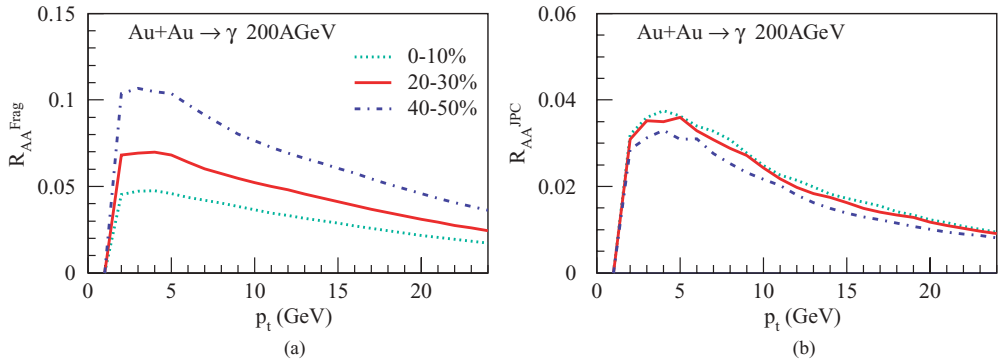

FIG. 10. (Color online) Contribution to R_{AA} from fragmentation and conversion, for different centralities.

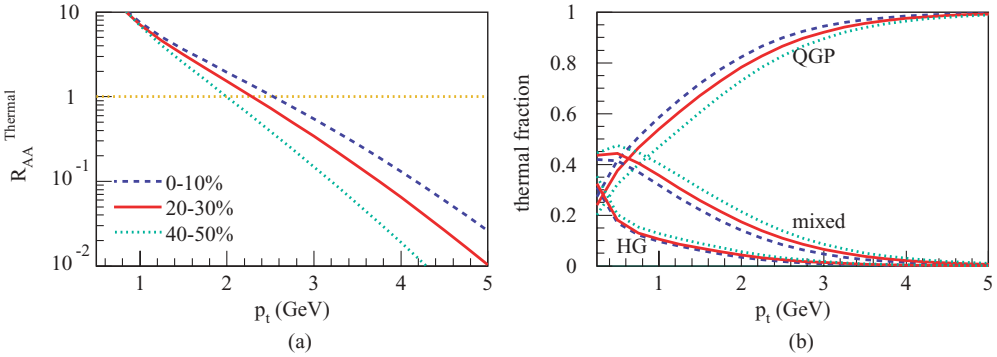

FIG. 11. (Color online) (a) Thermal contribution to R_{AA} from 0–10% (dashed line), 20–30% (solid line), and 40–50% (dotted line). (b) Fractions of thermal photon yields from the QGP, mixed, and HG phases.

the PCE, the chemical potential μ_i for all hadronic species i will modify the photon emission rate from hadronic gas, roughly estimated by a factor of $\exp[(\mu_1 + \mu_2)/T]$ for a subprocess of $1 + 2 \to 3 + \gamma$ according to kinetic theory with Maxwell-Boltzmann statistics for all particles. This factor finally increases the contribution from the HG by a factor of about 2. Nevertheless, in the total thermal contribution, PCE or FCE consideration does not make a visible difference. For all centralities from 0–10% to 50–60%, the QGP phase emits most of direct photons above $p_t \sim 1$ GeV/c. Although the volume of hadronic phase is much bigger than that of the QGP phase because of expansion, the photon emission rate from the hadronic phase decreases even faster with temperature. The competition between volume and emission rate results in the biggest contribution from the QGP phase at $p_t > 1$ GeV/c. In the current setting of hydrodynamic simulations at the RHIC energy $\sqrt{s_{NN}} = 200$ GeV, the mixed phase exists for a very long time (∼8 fm/c). This contributes mostly at lower p_t values. By combining the results shown in Figs. 9 and 11, contribution of thermal radiation from the QGP phase is dominant in the region $1 \lesssim p_t \lesssim 4$ GeV/c. This momentum window may provide information inside the hot and dense matter, e.g., the initial temperature at the center, which may not be reached directly by hadron spectra.

VI. CONCLUSION

We calculated the centrality dependence of p_t spectra for direct photons in Au + Au collisions at the RHIC energy $\sqrt{s_{NN}} = 200$ GeV, based on a realistic data-constrained (3 + 1)-D hydrodynamic description of the expanding hot and dense matter, a reasonable treatment of propagation of partons and their energy loss, and a systematic consideration of the main sources of direct photons. In this study, four main sources are considered: leading order (LO) contribution from primordial elementary scatterings, thermal radiation from the fluids, fragmentation from hard partons, and jet-photon conversion (JPC). Similar work [43] has been done before the appearance of the most recent data [41]. Our results agree nicely with the recent low p_t data.

The role of jet quenching in the high p_t region of direct photons production has been checked via fragmentation photons and jet-photon conversion sources. For these two sources, the suppression of the photon rate due to parton energy loss is significant in central Au + Au collisions, and it becomes less important toward peripheral collisions, similar to the suppression for meson production. Since experimentally one may separate isolated photons (LO + JPC) and associate photons (fragmentation photons), our prediction may be tested in the future.

Considering the total yields of direct photons, the contributions from fragmentation and conversion are small, contributing between 5% and 10%. However, parton energy loss plays nevertheless an important role. Without it, these second-order effects would contribute significantly. Without jet quenching, the nuclear modification factors R_{AA} would depend visibly on the centrality of the collisions. A strong energy loss is actually necessary to get the centrality scaling of R_{AA} in our calculation—a centrality scaling that has observed by the PHENIX Collaboration. In this sense, properties of the bulk matter affect the photon yields at intermediate values of p_t, via the parton energy loss.

The low p_t region is totally dominated by thermal radiation, providing direct information about the bulk matter. We find that R_{AA} of photons at p_t values below 1 GeV/c is centrality independent. With increasing p_t, the R_{AA} for peripheral collisions drops much faster than the one for central scatterings. On the other hand, thermal photons are mainly emitted from the QGP phase at $p_t > 1$ GeV/c even though the mixed phase and the HG phase occupy bigger space and longer time. So the different behavior of R_{AA} for central and peripheral collisions, in the range $1 < p_t < 3$ GeV/c, manifests the fact that the plasma in central collisions is hotter than that in peripheral collisions.

Still more investigation is needed for a precise characterization of the properties of the plasma via thermal photons. Besides, the elliptic flow of direct photons (especially thermal photons) should provide more information on the plasma, which will be discussed elsewhere.

ACKNOWLEDGMENTS

This work is supported by the Natural Science Foundation of China under Project No. 10505010 and MOE of China under

Project No. IRT0624. The work of T.H. was partly supported by Grant-in-Aid for Scientific Research No. 19740130. F.M.L. thanks the IN2P3/CNRS and Subatech for their hospitality during her visit in Nantes. T.H. and K.W. thank the Institute of Particle Physics, Central China Normal University for its hospitality during their visits.

[1] *Proceedings of Quark Matter 2006*, J. Phys. G: Nucl. Part. Phys. **34** (2007).
[2] J. W. Harris and B. Muller, Annu. Rev. Nucl. Part. Sci. **46**, 71 (1996).
[3] K. Adcox *et al.* (PHENIX Collaboration), Phys. Rev. Lett. **88**, 022301 (2002); S. S. Adler *et al.* (PHENIX Collaboration), *ibid.* **91**, 072301 (2003); C. Adler *et al.* (STAR Collaboration), *ibid.* **89**, 202301 (2002); **90**, 082302 (2003).
[4] J. D. Bjorken, FERMILAB-PUB-82-059-THY (unpublished).
[5] M. Gyulassy and M. Plumer, Phys. Lett. **B243**, 432 (1990); X. N. Wang and M. Gyulassy, Phys. Rev. Lett. **68**, 1480 (1992).
[6] R. Baier, Y. L. Dokshitzer, A. H. Mueller, S. Peigne, and D. Schiff, Nucl. Phys. **B483**, 291 (1997); **B484**, 265 (1997).
[7] R. Baier, D. Schiff, and B. G. Zakharov, Annu. Rev. Nucl. Part. Sci. **50**, 37 (2000); U. Wiedemann, Nucl. Phys. **B588**, 303 (2000).
[8] B. B. Back *et al.* (PHOBOS Collaboration), Phys. Rev. Lett. **91**, 072302 (2003); S. S. Adler *et al.* (PHENIX Collaboration), *ibid.* **91**, 072303 (2003); J. Adams *et al.* (STAR Collaboration), *ibid.* **91**, 072304 (2003); I. Arsene *et al.* (BRAHMS Collaboration), *ibid.* **91**, 072305 (2003).
[9] A. Adare *et al.* (PHENIX Collaboration), Phys. Rev. Lett. **101**, 232301 (2008).
[10] T. Hirano, Phys. Rev. C **65**, 011901(R) (2001).
[11] T. Hirano and K. Tsuda, Phys. Rev. C **66**, 054905 (2002).
[12] S. Turbide, C. Gale, S. Jeon, and G. D. Moore, Phys. Rev. C **72** 014906 (2005).
[13] C. Gale, Nucl. Phys. **A785**, 93 (2007).
[14] B. G. Zakharov, JETP Lett. **80**, 1 (2004) [Pis'ma Zh. Eksp. Teor. Fiz. **80**, 3 (2004)].
[15] P. Braun-Munzinger, D. Magestro, K. Redlich, and J. Stachel, Phys. Lett. **B518**, 41 (2001).
[16] H. Bebie, P. Gerber, J. L. Goity, and H. Leutwyler, Nucl. Phys. **B378**, 95 (1992).
[17] N. Arbex, F. Grassi, Y. Hama, and O. Socolowski Jr., Phys. Rev. C **64**, 064906 (2001); W. L. Qian, R. Andrade, F. Grassi, Y. Hama, and T. Kodama, arXiv:0709.0845 [nucl-th].
[18] D. Teaney, nucl-th/0204023.
[19] P. F. Kolb and R. Rapp, Phys. Rev. C **67**, 044903 (2003).
[20] P. Huovinen, Eur. Phys. J. A **37** 121 (2008).
[21] T. Hirano, U. Heinz, D. Kharzeev, R. Lacey, and Y. Nara, Phys. Lett. **B636**, 299 (2006); J. Phys. G **34**, S879 (2007); Phys. Rev. C **77**, 044909 (2008).
[22] B. B. Back *et al.* (PHOBOS Collaboration), Phys. Rev. C **65**, 061901 (2002).
[23] T. Hirano and Y. Nara, Phys. Rev. C **68**, 064902 (2003); **69**, 034908 (2004); Phys. Rev. Lett. **91**, 082301 (2003); M. Isse *et al.*, Int. J. Mod. Phys. E **16**, 2338 (2007); T. Gunji, H. Hamagaki, T. Hatsuda, and T. Hirano, Phys. Rev. C **76**, 051901(R) (2007); T. Hirano, in Proceedings of Hard Probes 2008, Eur. Phys. J. C (to be published).
[24] J. F. Owens, Rev. Mod. Phys. **59**, 465 (1987).
[25] A. D. Martin, R. G. Roberts, W. J. Stirling, and R. S. Thorne, Eur. Phys. J. C **23**, 73 (2002).
[26] K. J. Eskola, V. J. Kolhinen, and C. A. Salgado, Eur. Phys. J. C **9**, 61 (1999); K. J. Eskola, V. J. Kolhinen, and P. V. Ruuskanen, Nucl. Phys. **B535**, 351 (1998).
[27] F. Karsch, Z. Phys. C **38**, 147 (1988).
[28] M. Gyulassy and X.-N. Wang, Nucl. Phys. **B420**, 583 (1994).
[29] B. A. Kniehl, G. Kramer, and B. Potter, Nucl. Phys. **B597**, 337 (2001).
[30] A. Adare *et al.* (PHENIX Collaboration), Phys. Rev. D **76**, 051106 (2007).
[31] X. N. Wang, Phys. Lett. **B595**, 165 (2004); **B570**, 299 (2004).
[32] J. Kapusta, P. Lichard, and D. Seibert, Phys. Rev. D **44**, 2774 (1991); **47**, 4171(E) (1991).
[33] R. Baier, H. Nakkagawa, A. Niegawa, and K. Redlich, Z. Phys. C **53**, 433 (1992).
[34] P. Arnold, G. D. Moore, and L. G. Yaffe, J. High Energy Phys. 11 (2001) 057; 12 (2001) 009.
[35] S. Turbide, R. Rapp, and C. Gale, Phys. Rev. C **69**, 014903 (2004); C. Song, *ibid.* **47**, 2861 (1993).
[36] F. Arleo *et al.*, hep-ph/0311131; R. Rapp and C. Gale, Phys. Rev. C **60**, 024903 (1999).
[37] C. Y. Wang, *Introduction to High-Energy Heavy Ion Collisions* (World Scientific, Singapore, 1994).
[38] R. J. Fries, B. Muller, and D. K. Srivastava, Phys. Rev. Lett. **90**, 132301 (2003); Phys. Rev. C **72**, 041902(R) (2005).
[39] Tadaaki Isobe *et al.* (PHENIX Collaboration), J. Phys. G **34**, S1015 (2007).
[40] S. S. Adler *et al.* (PHENIX Collaboration), Phys. Rev. Lett. **98**, 012002 (2007).
[41] A. Adare *et al.* (PHENIX Collaboration), arXiv:0804.4168 [nucl-ex].
[42] S. S. Adler *et al.* (PHENIX Collaboration), Phys. Rev. Lett. **94**, 232301 (2005).
[43] S. Turbide, C. Gale, E. Frodermann, and U. Heinz, Phys. Rev. C **77**, 024909 (2008).